Desalination and Water Treatment
www.deswater.com
doi: 10.5004/dwt.2022.28291

253 (2022) 39–47
March

Preparation of plant-polyphenolic polyvinylidene fluoride nanocomposite membrane and its application in simulated Reactive black 5 wastewater treatment

Zeyuan Jiang, Rui Tao, Honghai Yang*, Jun Wang*

College of Environmental Science and Engineering, Donghua University, 2999 North Renmin Road, Shanghai, China, Tel. +86-21-67792539; emails: yhh@dhu.edu.cn (H. Yang), wangj@dhu.edu.cn (J. Wang), 1356863921@qq.com (Z. Jiang), 1137313225@qq.com (R. Tao)

Received 18 October 2021; Accepted 3 February 2022

ABSTRACT

The preparation of nanofiltration membranes with good separation performance and stability for dye wastewater treatment is imperative. The composite nanofiltration membrane prepared by the method of interfacial polymerization usually have the drawback of the instability. The selective layer inclined to peel off the substrate due to the weak adhesion between the selective layer and the substrate. In this work, inspired by polyphenol chemistry, polyethylenimine (PEI) was co-deposited with the mixture of tannic acid (TA) and gallic acid (GA), on the surface of polyvinylidene fluoride ultrafiltration membrane, then a nanometers thickness polyamide selective layer was formed by the interfacial polymerization of PEI and homophthaloyl chloride. The chemical structure, surface roughness, microstructure and hydrophilicity of the surface of the selective layer of the composite nanofiltration membrane were characterized by Fourier-transform infrared spectroscopy, atomic force microscopy, scanning electron microscopy, and water contact angle meter, respectively. The present work focused on the effects of the ratio of TA to GA on the performance and structure of the selective layer. Lastly, the performance and stability of the prepared nanocomposite membranes in the simulating Reactive black 5 (RB5) dyeing wastewater treatment were investigated. The results showed that: the surface roughness, the thickness and the water contact angle of the selective layer and the water flux all tended to decline and the polyethylene glycol (PEG1000) rejections kept being above 97% with the ratio of TA to GA decrease; the change of the dye effluent flux, the RB5 and the salt rejection were similar to that of the water flux and PEG1000, the RB5 rejection had being kept above 91%, the separation factor of dye and salt was up to 12.97, the prepared nanocomposite membranes displayed good operational stability within operating time.

Keywords: Nanocomposite membranes; Polyvinylidene fluoride; Tannic acid/Gallic acid; Co-deposition; Interfacial polymerization

1. Introduction

In recent years, the rapid development of the printing and dyeing industry brought more and more dyeing wastewater, which is highly toxic, difficult to degrade, and contains a large number of carcinogenic, teratogenic, and mutagenic organic compounds. The untreated dyeing wastewater discharged into water bodies would threaten humans health and also impede photosynthesis of plants in the water body, leading to a lack of oxygen in the water body' causing the deterioration of water quality. Traditional methods of removing dyes included advanced chemical oxidation, biodegradation, adsorption, coagulation and sedimentation. However, these methods have this and

* Corresponding authors.

that draw backs, for example, not up to standard, high cost, producing secondary pollution [1,2], etc. Therefore, it is important to develop an efficient and environmentally friendly treatment technology [3–6].

Nanofiltration (NF) has the advantages of high separation efficiency, low energy consumption and cost, compactness, simple equipment, and easy operation compared to conventional separation technologies such as adsorption and coagulation [7–9]. As a typical pressure-driven membrane separation process, NF can easily separate substances with molecular weights in the range of 200–1,000 Da from water and can produce high water fluxes at relatively low operating pressures [10,11], which has promising applications in the treatment of dye wastewater and is very suitable for the treatment of dye wastewater [12,13].

Currently, interfacial polymerization is the dominant technology for manufacturer-use and laboratory nanofiltration membranes, which include a polyamide selective layer attached to a porous matrix, which is typically an ultrafiltration or microfiltration membrane. However, the compatibility between the selector layer and the support layer may not be sufficient to confer satisfactory structural stability to the membrane under harsh conditions because there is no chemical bond between the two layers. To ensure the structural integrity of composite nanofiltration membranes and to impart attractive properties to the selector layer, surface coating with advanced functional building blocks on a porous substrate followed by in situ cross-linking has proven to be an effective strategy.

Tannic acid (TA) is widely found in plants and has attracted great attention in surface bio adhesive modification due to its low price and easy storage, and has been widely used in the preparation of composite nanofiltration membranes in recent years [14,15]. Gallic acid (GA) is a natural polyphenolic substance derived from tannin hydrolysis [16–18], which has a variety of biological activities such as anti-caries, antioxidant and antibacterial, and has a wide range of applications in food [19,20], pharmaceuticals, and other fields. TA and GA can produce strong adhesion to the material's substrate surface by building covalent and non-covalent bond structures after oxidizing a part of catechol to quinone under weak alkaline conditions. In addition, due to the presence of the quinone group, both TA and GA can form a composite coating with other substances on the membrane surface [21]. Polyethylenimine (PEI) is a hydrophilic polyelectrolyte with abundant amino groups [22]. Both TA and GA can be deposited on the membrane surface together with PEI through Michael addition/Schiff base reaction and non-covalent interactions to form a hydrophilic and strong selective layer.

In summary, to develop new nanofiltration membrane materials suitable for dye wastewater treatment, polyvinylidene fluoride (PVDF) ultrafiltration membrane was used as the base membrane in this work. Firstly, PEI was co-deposited with TA and GA on the surface of PVDF ultrafiltration membrane to generate a functionalized coating to immobilize PEI on the surface of PVDF ultrafiltration membrane, in addition, the amino-rich PEI was beneficial to neutralize the negative surface charge and significantly improve the coating, In addition, the amino-rich PEI helps to neutralize the negative surface charge and significantly improve the hydrophilicity of the coating, forming a loose and uniform surface structure. On this basis, the cross-linker homophthaloyl chloride (TMC) and PEI are used to generate a highly selective polyamide of nanometer thickness by interfacial polymerization, and the film will be firmly attached to the surface of the base membrane due to the adhesion of the functionalized coating. In addition, $CuSO_4$-$5H_2O$/H_2O_2 [23] was used as a self-polymerization initiator during the deposition process, and the resulting dense and smooth skin layer resulted in a nanofiltration membrane with high stability and effectively shortened the deposition time, such that a thin hydrophilic PA layer was formed in a relatively short period. The microstructure and properties of PA/TA/GA/PVDF composite nanofiltration membranes were studied using attenuated total reflection-Fourier-transform infrared spectroscopy (ATR-FTIR), scanning electron microscopy (SEM), atomic force microscopy (AFM), and water contact angles. The effects of TA/GA ratio on the structure and separation performance of PA/TA/GA/PVDF composite nanofiltration membranes were systematically investigated, which are of guidance for the practical application of nanofiltration membranes.

2. Experimental

2.1. Materials

MSC cup type ultrafilter (300 mL, Mosel Scientific Equipment Co., Ltd., China); field-emission scanning electron microscope (S-4800 type); atomic force microscope (AFM, Agilent-S5500, China); ultraviolet-visible spectrophotometer (UV-7504PC type); Fourier-transform infrared spectrometer (FTIR, FTS-6000 type); contact angle meter (JC2000C); TOC analyzer (TOC-5000A); polyvinylidene fluoride (PVDF, Shanghai Organic Fluorine Materials Co., Ltd., China); N,N-dimethylacetamide (DMAc, Sinopharm Chemical Reagent Co., Ltd., China, analytical purity); homophthaloyl chloride (TMC, 98%); copper sulfate pentahydrate ($CuSO_4 \cdot 5H_2O$, 99%, Sinopharm Chemical Reagent Co., Ltd., China); hydrogen peroxide (H_2O_2, 30%, Sinopharm Chemical Reagent Co., Ltd., China); Tris-HCl buffer stock solution (pH = 8.5, Bioengineering Co., Ltd., China); gallic acid (Rohn's Reagent, China). Tannic acid (Shanghai Maclean Biochemical Technology Co., Ltd. China); *n*-hexane (Sinopharm Chemical Reagent Co., Ltd., China, analytical purity); polyethylenimine (PEI, Sinopharm Chemical Reagent Co., Ltd., China); polyvinylpyrrolidone (PVP K30, Sinopharm Chemical Reagent Co., Ltd., China).

2.2. Fabrication of composite NF membranes

PVDF (18%), PVP (4%), and DMAc were proportionally heated and stirred in a thermostatic water bath at a certain temperature until completely dissolved, and left to degass. The finished degass cast film solution was poured onto a clean, dry glass plate, scraped into a film of certain thickness with a glass rod, then immediately dipped into a gel bath at a certain temperature, removed after its film formation, soaked in distilled water for more than 24 h to remove the solvent, dried and set aside.

Tannic acid and gallic acid were dissolved in a buffer containing $CuSO_4 \cdot 5H_2O$ (0.024 g) (10 mL, pH = 8.5), 40 μL

of 30% H_2O_2 was added, and mixed with aqueous PEI solution (10 mL). The mixed solution was poured on the fixed PVDF base membrane and co-deposited for a while, the membrane was removed to remove the residual solution on the surface and dried under ventilated conditions. The membranes were then immersed in a solution containing 0.2% w/v TMC hexane for 5 min, removed, and further dried under-ventilated conditions, and the dosage and reaction time of different drugs are shown in Table 1.

2.3. Membrane characterization

2.3.1. Characterization of chemical structure of nanofiltration membranes

ATR-FTIR was used to analyze the surface chemical structure of nanofiltration membranes. The IR spectrograms obtained from substance analysis reflect the type of functional groups contained in the substance, and the structure of the compound can be determined by analysis of the characteristic spectrum and fingerprint region degree [24]. To measure the infrared spectra of GA and PEI by the potassium bromide press method, the oven-dried potassium bromide is first ground into a powder in a mortar, and then the sample to be measured is added and ground thoroughly, and the sample is pressed into a tablet to be used for the infrared spectra measurement. To measure PA/TA/GA/PVDF films by IR probe method, the prepared samples were freeze-dried and cut to the right size. Then measured by FTIR spectroscopy.

2.3.2. Microstructure characterization of nanofiltration membrane

The prepared nanofiltration membranes were cut into 2 cm × 2 cm squares and the effect of different TA/GA ratios on the surface microstructure of PA/TA/GA/PVDF composite nanofiltration membranes were observed using field-emission scanning electron microscopy (FE-SEM). The surface roughness of PA/TA/GA/PVDF composite nanofiltration membranes was analyzed using AFM.

2.3.3. Hydrophilicity characterization of nanofiltration membrane

A contact angle measuring instrument was used to measure the water contact angle of the PA/TA/GA/PVDF composite nanofiltration membrane to characterize the hydrophilicity of the membrane, if the contact angle is less than 90°, the surface of the nanofiltration membrane is hydrophilic, that is, the liquid is easier to wet, and the smaller the angle, the better the wettability is; if the contact angle is greater than 90°, it is hydrophobic. The dried nanofiltration membrane was cut into a suitable size and pasted on a clean glass plate, and after adjusting the angle, the glass plate was placed under the contact angle tester and measured by the distilled water static drop method with a drop volume of 2 μL, so that the droplets fell on the sample surface. Adjust the position of the baseline where the droplet meets the sample, get the test result, and record the data.

2.3.4. Nanofiltration membrane filtration performance characterization

PA/PDA/PVDF composite nanofiltration membrane filtration performance including pure water throughput and MWCO.

Determination of pure water flux of PA/TA/GA/PVDF composite nanofiltration membrane. The nanofiltration membranes were cut into circular membrane pieces of appropriate size and placed in an ultrafiltration cup. The pure water flux of the nanofiltration membrane was measured at 0.1 MPa after 30 min of pre-pressure at 0.15 MPa, and the volume of the filtrate obtained by filtration was recorded at a certain time (data recorded every 10 min for 1 h) to calculate the pure water flux. The water flux was calculated as shown in Eq. (1).

$$J_w = \frac{V}{At} \tag{1}$$

where J_w is the water flux, L/m²·h; V is the volume of filtrate, L; A is the effective area of the membrane, 36.6 × 10^{-4} m²; t is the time h required to obtain V volume of filtrate.

PA/TA/GA/PVDF composite nanofiltration membrane cut-off molecular weight characterization: the retention molecular weight of the membrane is the molecular weight of the membrane when the retention rate of a constant molecular weight substance reaches 90%. The retention molecular weight of the PA/TA/GA/PVDF composite nanofiltration membrane is characterized by polyethylene glycol (PEG) with a molecular weight of 1,000 Da. A 1 g/L PEG

Table 1
Drug dosage and reaction time

TA/GA	TA (g/L)	GA (g/L)	PEI (g/L)	TMC (w/v)	Cross-linking time (min)	Deposition time (min)
10:0	0.75	0	2.25	0.2%	5	60
8:2	0.6	0.15	2.25	0.2%	5	60
6:4	0.45	0.3	2.25	0.2%	5	60
4:6	0.3	0.45	2.25	0.2%	5	60
2:8	0.15	0.6	2.25	0.2%	5	60
0:10	0	0.75	2.25	0.2%	5	60

solution was used to determine the MWCO of the membrane. The retention rate was determined using a TOC analyzer, and the inlet and outlet liquid total organic carbon values were measured using a TOC analyzer to derive the MWCO. The retention rate was calculated using Eq. (2):

$$R = \left(\frac{C_p - C_f}{C_p} \right) \times 100\% \quad (2)$$

where R is the retention rate, %; C_p and C_f are the concentration of the stock solution and filtrate, mg/L.

2.3.5. Characterization of filtration performance of nanofiltration membrane in dye wastewater

PA/TA/GA/PVDF composite nanofiltration membrane filtration performance including dye flux and dye retention PA/TA/GA/PVDF composite nanofiltration membrane dye flux was determined. The nanofiltration membranes were cut into circular membrane pieces of appropriate size and placed in an ultrafiltration cup. The dye flux of the nanofiltration membrane was measured at 0.1 MPa after 30 min of pre-pressure with pure water at 0.15 MPa, and the volume of the filtrate was obtained by filtration at a certain time (data recorded every 10 min for 1 h) was recorded to calculate the dye flux. The formula for calculating the dye flux is shown in Eq. (1).

The absorbance of the water sample was measured using a UV-7504PC UV-Vis spectrophotometer and the dye retention was calculated according to Eq. (3).

$$R_1 = \left(\frac{C_0 - C}{C_0} \right) \times 100\% \quad (3)$$

where R_1 is the retention rate; C_0 is the concentration of the dye before treatment and C is the concentration of the dye filtrate after treatment.

The retention of salt by the composite nanofiltration membrane was characterized by measuring the conductivity of the stock and filtrate by a conductivity meter, and the salt retention was calculated using Eq. (4):

$$R_2 = \left(\frac{\sigma_0 - \sigma}{\sigma_0} \right) \times 100\% \quad (4)$$

where R_2 is the salt retention rate, %; σ_0 and σ are the conductivity of the stock solution and filtrate, S/m.

The separation factor of dye and salt was calculated using Eq. (5) to calculate the ratio of dye and salt retention.

$$K_{\text{dye/salt}} = \frac{R_1}{R_2} \quad (5)$$

2.3.6. Stability of composite nanofiltration membranes in Reactive black 5 dye wastewater

The simulated dye wastewater was filtered at 0.1 MPa after 30 min of pre-pressure at 0.15 MPa, and the volume of filtrate was recorded every 30 min for 6 h. The flux was calculated using Eq. (1), and the dye retention rate was calculated using Eq. (3). The filtration stability of the composite nanofiltration membrane on simulated dye wastewater was tested.

3. Results and discussion

3.1. Qualitative analysis of infrared spectrum of nanofiltration membrane

The chemical structure of the membrane surface was investigated by ATR-FTIR analysis. It can be seen from Fig. 1 that the PA/TA/GA/PVDF composite nanofiltration membrane and PVDF membrane found the characteristic peak at 1,000–1,400 cm^{-1}, which belongs to the absorption vibration of the C–F bond [25]. The characteristic peaks of TA and PEI appeared in 3,200–3,500 cm^{-1}, belonging to the amino peak. The characteristic peak of GA was found at 3,492 cm^{-1}, which indicates that the formed PA layer is attached to the PVDF base membrane, and it should be pointed out that GA is soluble in water, the GA residue was easily removed by the water washing step of the post-treatment, ruling out the possibility of free GA physically adsorbed on the PVDF base film surface [26–29]. The composite nanofiltration membrane has a new peak at 1,660 cm^{-1}, which is the overlap of C=C resonance vibration and C=N tensile vibration in the aromatic ring, confirming the existence of PA layer on the PVDF-based membrane.

3.2. Effect of TA/GA ratio on microstructure of nanofiltration membrane

The surface morphology, the thickness and the roughness of the selective layer play crucial role in the separation performance of nanocomposite membranes. Fig. 2 shows effects of the ratio of TA to GA on the SEM and AFM images of PA/TA/GA/PVDF nanocomposite membranes. As shown in the figure, the membrane surface has more nodular prominence and be more roughness when the content of TA in the mixture of TA and GA was much greater. For example, when the value of TA/GA was 10/0, the surface roughness

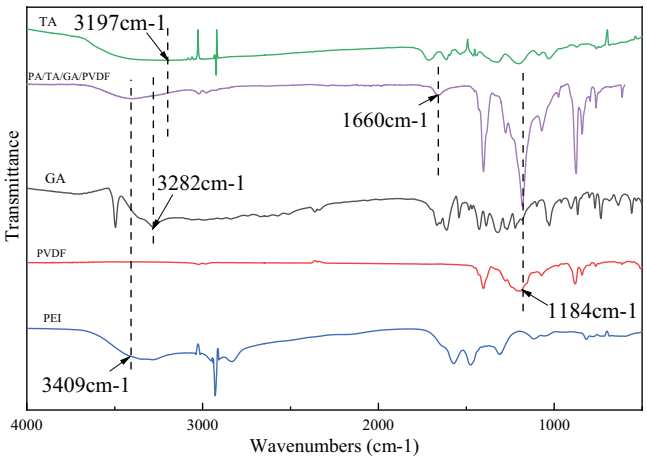

Fig. 1. Infrared spectra of GA, TA, PVDF, PEI, PA/TA/GA/PVDF composite nanofiltration membranes (ATR-FTIR).

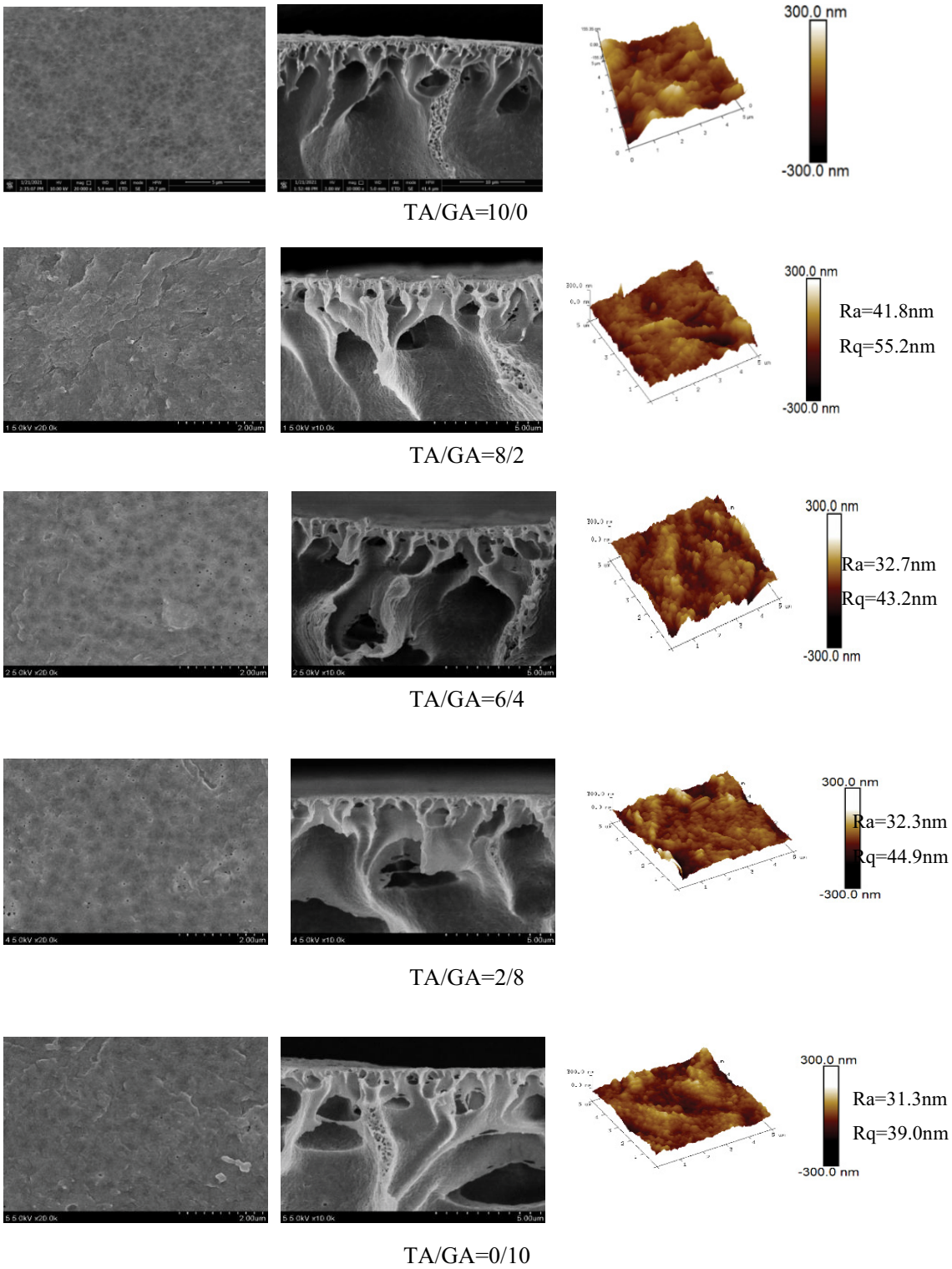

Fig. 2. Effect of TA/GA ratio on microstructure of PA/TA/GA/PVDF composite nanofiltration membrane (SEM, AFM images).

was Ra = 45.7 nm and Rq = 55.9 nm. However, when the value of TA/GA was 0/10, the surface roughness was only Ra = 31.3 nm and Rq = 39.0 nm. On the other hand, with the TA content increases, the thickness of the selective layer tend to become thicker and more porous. The increase of the surface roughness could lead to the increase of the effective filtration area. Above results were due to that TA has more hydroxyl groups than GA, and replacing part of GA

with TA, the reaction with PEI is more intense [30], so more aggregates are produced on the membrane surface making the roughness of the membrane surface higher [31,32]. In addition, the molecular of TA is much larger than that of GA, which makes the molecular volume of TA is much larger than that of the GA.

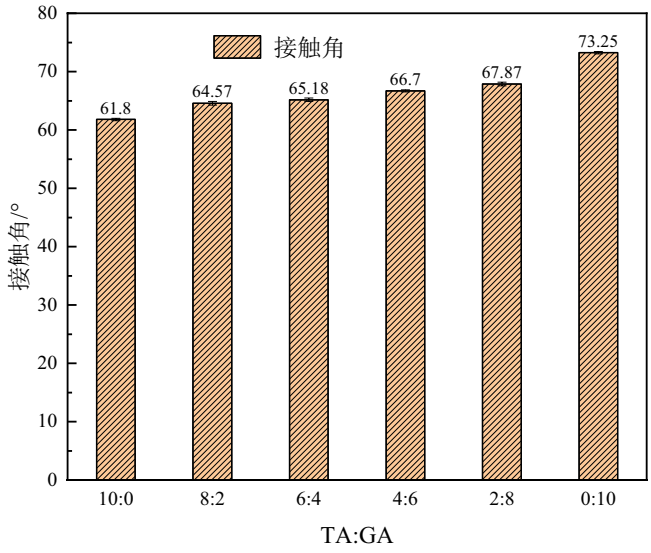

Fig. 3. Effect of TA/GA ratio on the water contact angle of PA/TA/GA/PVDF.

3.3. Effect of TA/GA ratio on hydrophilicity of nanofiltration membrane

Fig. 3 shows the variation of water contact angle of PA/TA/GA/PVDF composite nanofiltration membrane with different ratios of TA/GA, and the hydrophilicity of the membrane showed a wave-like decreasing trend as the ratio of TA/GA decreased [33]. This is because TA has abundant hydrophilic hydroxyl groups, which help to reduce the water contact angle on the membrane surface, so the water contact angle of PA/TA/GA/PVDF composite nanofiltration membrane becomes larger and the hydrophilicity decreases as the ratio of TA decreases. Because of the stochastic nature of the chemical reaction, the water contact angle shows a decreasing trend for a period during the increase [34–37].

3.4. Filtration performance of nanofiltration membranes

The effect of the ratio of TA to GA on the pure water flux and the PEG1000 rejection are shown in Fig. 4a. Fig. 4b shows the change the pure water flux within 1 h. Fig. 4a displays that the water flux increased slowly firstly, then decreased quickly with the decrease of ratio of TA to GA. The water flux was up to the maximum value at the ratio of TA to GA of 6/4. The rejection of PEG1000 changed little in the range of ratio of TA to GA. These variation were related to the difference of the molecular volume and the number of hydroxyl groups between TA and GA. The molecular weight of TA is 1,701.3 Da and that of GA is 170.1, so the TA has larger

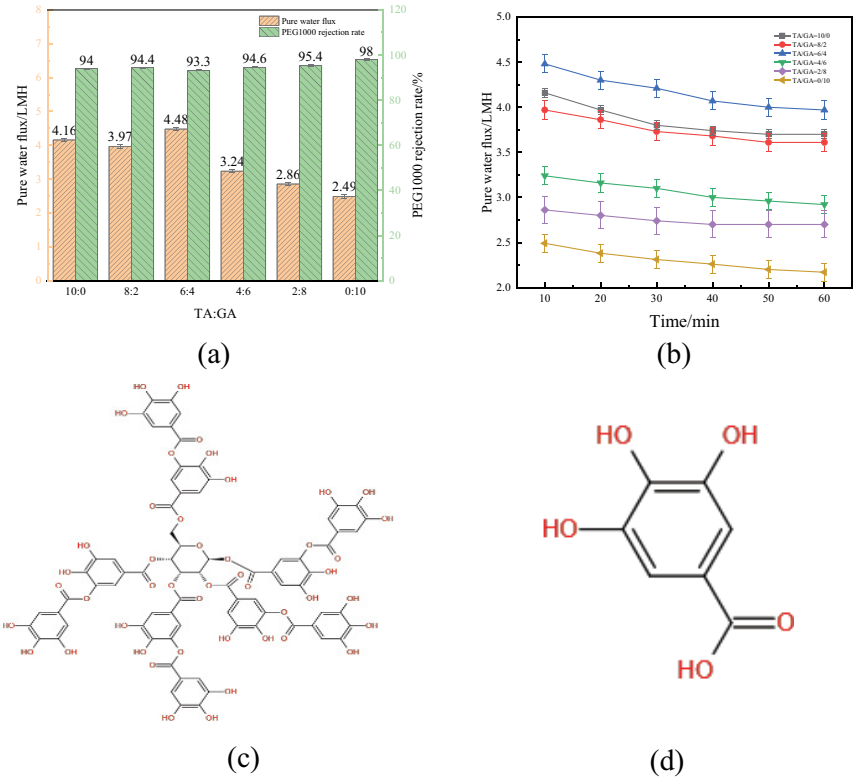

Fig. 4. (a) Effect of TA/GA value on the pure water flux and PEG1000 rejection of the composite nanofiltration membrane. (b) Effect of TA/GA value on the pure water flux every 10 min of the composite nanofiltration membrane. Molecular structure diagram of (c) TA and (d) GA.

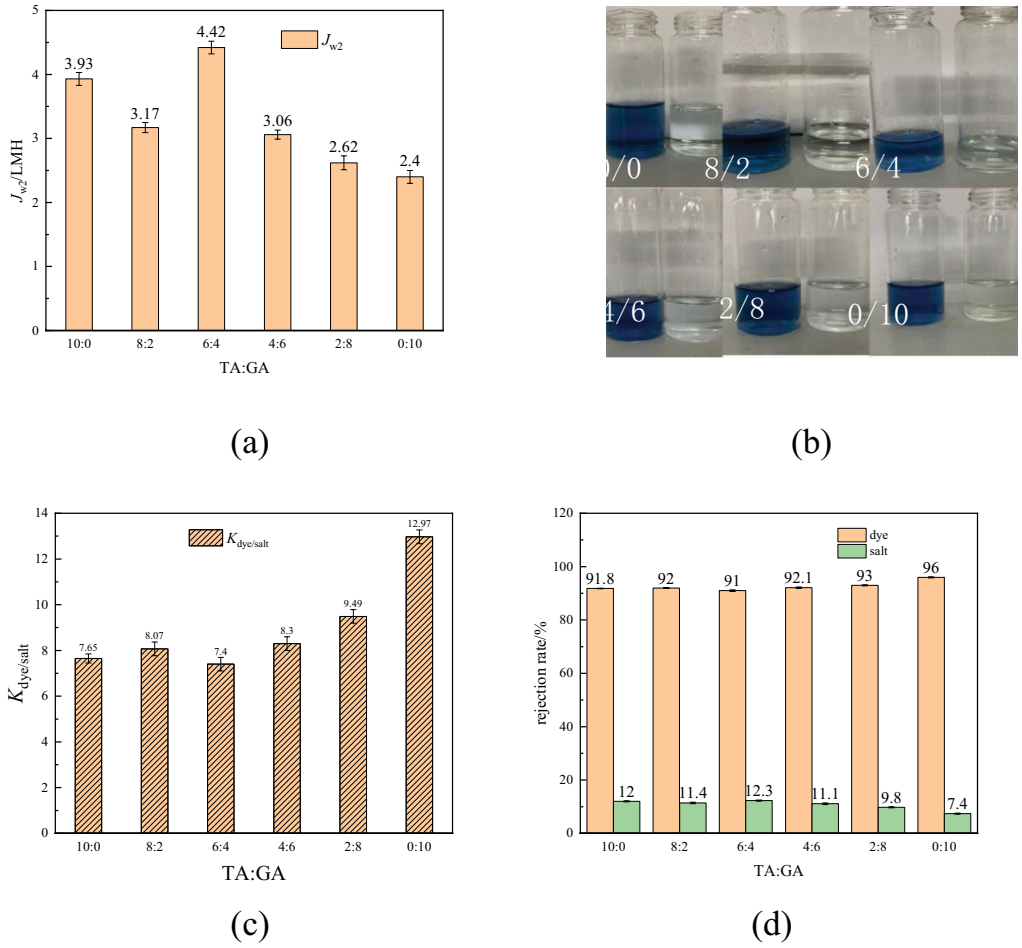

Fig. 5. (a) Effect of TA/GA ratio on the flux of composite nanofiltration membrane in RB5 wastewater. (b) Effect of dye retention (left: stock solution, right: filtrate). (c) Effect of TA/GA ratio on separation factor of dyes and salts ($K_{dye/salt}$). (d) Effect of TA/GA ratio on retention of dyes and salts.

molecular volume. The TA incline to form relative larger channel than the GA in the selective layer. However, mixing GA with TA properly can condition the number and size of the channel. On the other hand, TA molecular has much more hydroxyl groups than GA molecular as shown in Fig. 4c and d, which make the selective layer more hydrophilic when the content of TA is greater than that of GA.

3.5. Performance of nanofiltration membrane in Reactive black 5 simulated dye wastewater

3.5.1. Effects of TA/GA values on the dye solution flux and the rejection Reactive black 5 and salt

Reactive black 5 (RB5) is a common reactive dye in printing and dyeing textile industry. RB5 is very toxic, and it is difficult to degrade once discharged into water, which seriously damages human health. Fig. 5a and d show the effect of the TA/GA ratio on the flux and retention of RB5 dye treated by the PA/TA/GA/PVDF composite nanofiltration membrane. The retention of RB5 by membranes with ratios of 10/0, 8/2, 6/4,4/6, 2/8, and 0/10 were 91.8%, 92%, 91%, 92.1%, 93%, and 96%, respectively, and the dye flux reached a maximum while the retention rate reached a minimum at the ratio of 6/4. With the increase of GA, the dye flux showed a wave-like decrease, which was since TA had more hydroxyl groups than GA, and the total hydroxyl groups decrease after replacing a part of TA with GA, which makes the PEI content relatively increase, and the increase of PEI content will make more amine monomers participate in the reaction to make PEI cross-linked with TMC, and the interfacial polymerization is obvious, and the thickness of polyamide selective layer increases, which makes the dye flux decrease. However, the chemical reaction has randomness, so the dye flux showed an upward trend in one period during the decline. 6 composite nanofiltration membranes achieved more than 90% retention of RB5 solution, reaching the nanofiltration membrane level. The dye retention effect graph is shown in Fig. 5b. In addition, from Fig. 5a, it can also be found that the flux of the PA/TA/GA/PVDF composite nanofiltration membrane for the dye solution is significantly lower than the flux of purer water, which is due to the increased filtration resistance caused by the dye retained on the membrane surface during the filtration process of the dye solution.

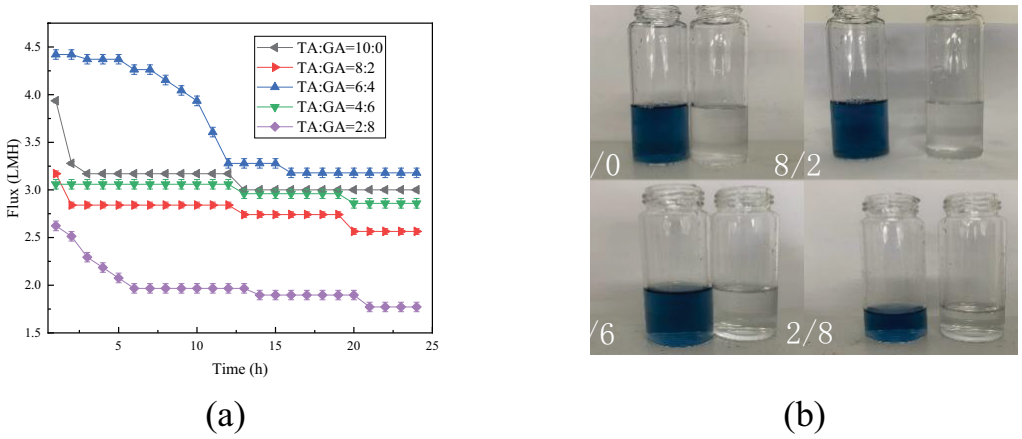

Fig. 6. (a) Dye flux stability of PA/TA/GA/PVDF composite nanofiltration membrane RB5 and (b) effect of dye retention (left: stock solution, right: filtrate).

From Fig. 5d it can be found that the retention of salt by PA/TA/GA/PVDF composite nanofiltration membrane shows a wave-like decreasing trend as the TA ratio decreases, and this changing trend is consistent with the changing trend of the flux and PEG1000 retention of pure water by PA/TA/GA/PVDF composite nanofiltration membrane for the reasons mentioned above. The results in Fig. 5 show that the PA/TA/GA/PVDF composite nanofiltration membrane decreases the retention capacity of salt with the decrease of TA ratio, thus the separation factor of dye and salt is increased and the treatment effect of dye wastewater is improved.

3.6. Stability of composite nanofiltration membrane

Stability is a very important factor in the reagent application of nanofiltration membranes. The stability of PA/TA/GA/PVDF composite nanofiltration membrane with different ratios of TA:GA was tested for 24 h using RB5 solution, and the results are shown in Fig. 6. The flux of RB5 solution showed a decreasing trend and then stabilized, and the RB5 retention rate was kept above 90% during the experiment, and the PA/TA/GA/PVDF composite nanofiltration membrane in dye separation showed good stability and separation performance.

4. Conclusions

Through the above results and discussions, the following conclusions can be obtained: when TA and GA are used as mixed plant polyphenols to prepare PA/TA/GA/PVDF composite nanofiltration membrane, when the TA content is higher, the membrane surface roughness, hydrophilicity, pure water flux and dye solution flux are higher than those when the GA content is higher; when TA:GA was 6:4, the membrane water flux and dye solution flux reached the maximum; PA/TA/GA/PVDF composite nanofiltration membrane for dye RB5 rejection rate is more than 90%, the rejection rate of salt is less than 12%, dye and salt can be separated to a large extent, the separation factor is more than 7.0; during the operation time, the PA/TA/GA/PVDF composite nanofiltration membrane showed good operation stability in the simulation of RB5 and NaCl dye wastewater treatment.

References

[1] D. Guo, Y. Xiao, T. Li, Q. Zhou, L. Shen, R. Li, Y. Xu, H. Lin, Fabrication of high-performance composite nanofiltration membranes for dye wastewater treatment: mussel-inspired layer-by-layer self-assembly, J. Colloid Interface Sci., 560 (2020) 273–283.
[2] F. Soyekwo, C. Liu, H. Wen, Y. Hu, Construction of an electroneutral zinc incorporated polymer network nanocomposite membrane with enhanced selectivity for salt/dye separation, Chem. Eng. J., 380 (2020) 122560, doi: 10.1016/j.cej.2019.122560.
[3] N.C. Homem, N. de Camargo Lima Beluci, S. Amorim, R. Reis, A.M.S. Vieira, M.F. Vieira, R. Bergamasco, M.T.P. Amorim, Surface modification of a polyethersulfone microfiltration membrane with graphene oxide for reactive dyes removal, Appl. Surf. Sci., 486 (2019) 499–507.
[4] M.-L. Liu, L. Li, M.-J. Tang, L. Hong, S.-P. Sun, W. Xing, Multi-component separation of small molecular/ionic pollutants with smart pH-gating membranes, Chem. Eng. Sci., 245 (2021) 116854, doi: 10.1016/j.ces.2021.116854.
[5] M.Q. Seah, W.J. Lau, P.S. Goh, A.F. Ismail, Greener synthesis of functionalized-GO incorporated TFN NF membrane for potential recovery of saline water from salt/dye mixed solution, Desalination, 523 (2022) 115403, doi: 10.1016/j.desal.2021.115403.
[6] P. Manna, R. Bernstein, R. Kasher, Stepwise synthesis of polyacrylonitrile-supported oligoamide membranes with selective dye–salt separation, J. Membr. Sci., 643 (2022) 120035, doi: 10.1016/j.memsci.2021.120035.
[7] X.-L. Cao, Y.-N. Yan, F.-Y. Zhou, S.-P. Sun, Tailoring nanofiltration membranes for effective removing dye intermediates in complex dye-wastewater, J. Membr. Sci., 595 (2020) 117476, doi: 10.1016/j.memsci.2019.117476.
[8] D.-D. Shao, L. Wang, X.-Y. Yan, X.-L. Cao, T. Shi, S.-P. Sun, Amine–carbon quantum dots (CQDs–NH_2) tailored polymeric loose nanofiltration membrane for precise molecular separation, Chem. Eng. Res. Des., 171 (2021) 237–246.
[9] B. Yang, K. Gu, S. Wang, Z. Yi, Y. Zhou, C. Gao, Chitosan nanofiltration membranes with gradient cross-linking and improved mechanical performance for the removal of divalent salts and heavy metal ions, Desalination, 516 (2021) 115200, doi: 10.1016/j.desal.2021.115200.
[10] L. Chen, C. Zhang, A. Gao, J. Cui, Y. Yan, Nanofiltration membrane embedded with hydroxyapatite nanowires as

interlayer towards enhanced separation performance, Colloids Surf., A, 626 (2021) 127001, doi: 10.1016/j.colsurfa.2021.127001.
[11] L. Zhang, R. Zhang, M. Ji, Y. Lu, Y. Zhu, J. Jin, Polyamide nanofiltration membrane with high mono/divalent salt selectivity via pre-diffusion interfacial polymerization, J. Membr. Sci., 636 (2021) 119478, doi: 10.1016/j.memsci.2021.119478.
[12] X. Geng, J. Wang, Y. Ding, W. Zhang, Y. Wang, F. Liu, Poly(vinyl alcohol)/polydopamine hybrid nanofiltration membrane fabricated through aqueous electrospraying with excellent antifouling and chlorine resistance, J. Membr. Sci., 632 (2021) 119385, doi: 10.1016/j.memsci.2021.119385.
[13] S. Kiani, S.M. Mousavi, A. Bidaki, Preparation of polyethylene terephthalate/xanthan nanofiltration membranes using recycled bottles for removal of diltiazem from aqueous solution, J. Cleaner Prod., 314 (2021) 128082, doi: 10.1016/j.jclepro.2021.128082.
[14] Z. Rahimi, A.A. Zinatizadeh, S. Zinadini, M. van Loosdrecht, A hydrophilic and antifouling nanofiltration membrane modified by citric acid functionalized tannic acid (CA-f-TA) nanocomposite for dye removal from biologically treated baker's yeast wastewater, J. Environ. Chem. Eng., 9 (2021) 104963, doi: 10.1016/j.jece.2020.104963.
[15] F. Oulad, S. Zinadini, A.A. Zinatizadeh, A.A. Derakhshan, Fabrication and characterization of a novel tannic acid coated boehmite/PES high performance antifouling NF membrane and application for licorice dye removal, Chem. Eng. J., 397 (2020) 125105, doi: 10.1016/j.cej.2020.125105.
[16] T.N. Baite, B. Mandal, M.K. Purkait, Ultrasound assisted extraction of gallic acid from *Ficus auriculata* leaves using green solvent, Food Bioprod. Process., 128 (2021) 1–11.
[17] I.S. Martakov, O.G. Shevchenko, M.A. Torlopov, E.Yu. Gerasimov, P.A. Sitnikov, Formation of gallic acid layer on γ-AlOOH nanoparticles surface and their antioxidant and membrane-protective activity, J. Inorg. Biochem., 199 (2019) 110782, doi: 10.1016/j.jinorgbio.2019.110782.
[18] L. Xuan, L.-J. Tian, T. Tian, X.-M. Wang, D.-H. Yang, H.-Q. Yu, *In situ* synthesizing silver nanoparticels by bio-derived gallic acid to enhance antimicrobial performance of PVDF membrane, Sep. Purif. Technol., 251 (2020) 117381, doi: 10.1016/j.seppur.2020.117381.
[19] M. Sguizzato, G. Valacchi, A. Pecorelli, P. Boldrini, F. Simelière, N. Huang, R. Cortesi, E. Esposito, Gallic acid loaded poloxamer gel as new adjuvant strategy for melanoma: a preliminary study, Colloids Surf., B, 185 (2020) 110613, doi: 10.1016/j.colsurfb.2019.110613.
[20] P. Praveen Kumar, D. Madhuri, L. Siva Sankar Reddy, Y. Dastagiri Reddy, G. Somasekhar, N.V.L. Sirisha, K. Nagaraju, M.S. Shouib, A.S. Rizwaan, A new cerebral ischemic injury model in rats, preventive effect of gallic acid and in silico approaches, Saudi J. Biol. Sci., 28 (2021) 5204–5213.
[21] C. Li, X. Chen, J. Luo, F. Wang, G. Liu, H. Zhu, Y. Guo, PVDF grafted gallic acid to enhance the hydrophilicity and antibacterial properties of PVDF composite membrane, Sep. Purif. Technol., 259 (2021) 118127, doi: 10.1016/j.seppur.2020.118127.
[22] T.X.H. Le, M. Bechelany, J. Champavert, M. Cretin, A highly active based graphene cathode for the electro-Fenton reaction, RSC Adv., 5 (2015) 42536–42539.
[23] C. Zhang, Y. Ou, W.-X. Lei, L.-S. Wan, J. Ji, Z.-K. Xu, $CuSO_4$/H_2O_2-induced rapid deposition of polydopamine coatings with high uniformity and enhanced stability, Angew. Chem. Int. Ed. Engl., 128 (2016) 3106–3109.
[24] G. Zeng, Z. Ye, Y. He, X. Yang, J. Ma, H. Shi, Z. Feng, Application of dopamine-modified halloysite nanotubes/PVDF blend membranes for direct dyes removal from wastewater, Chem. Eng. J., 323 (2017) 572–583.
[25] W.Z. Qiu, Y. Lv, Y. Du, H.-C. Yang, Z.-K. Xu, Composite nanofiltration membranes via the co-deposition and cross-linking of catechol/polyethylenimine, RSC Adv., 6 (2016) 34096–34102.
[26] G. Zhang, P.G. Ranjith, Z. Li, J. Vongsvivut, M. Gao, Application of synchrotron ATR-FTIR microspectroscopy for chemical characterization of bituminous coals treated with supercritical CO_2, Fuel, 296 (2021) 120639, doi: 10.1016/j.fuel.2021.120639.
[27] L. Hssaini, R. Razouk, J. Charafi, K. Houmanat, H. Hanine, Fig seeds: combined approach of lipochemical assessment using gas chromatography and FTIR-ATR spectroscopy using chemometrics, Vibr. Spectros., 114 (2021) 103251, doi: 10.1016/j.vibspec.2021.103251.
[28] X. Yang, X. Wei, K. Yu, C. Wan, Y. Wang, S. Huang, Q. Sun, J. Huang, Identification of myocardial fibrosis by ATR-FTIR spectroscopy combined with chemometrics, Spectrochim. Acta, Part A, 264 (2022) 120238, doi: 10.1016/j.saa.2021.120238.
[29] L. Luo, L. Xu, J. Meng, J. Lu, H. Wu, New insights into the mixed anionic/cationic collector adsorption on ilmenite and titanaugite: an in situ ATR-FTIR/2D-COS study, Miner. Eng., 169 (2021) 106946, doi: 10.1016/j.mineng.2021.106946.
[30] P. Jin, J. Zhu, S. Yuan, G. Zhang, A. Volodine, M. Tian, J. Wang, P. Luis, B. Van der Bruggen, Erythritol-based polyester loose nanofiltration membrane with fast water transport for efficient dye/salt separation, Chem. Eng. J., 406 (2021) 126796, doi: 10.1016/j.cej.2020.126796.
[31] J. Chau, K.K. Sirkar, K.J. Pennisi, G. Vaseghi, L. Derdour, B. Cohen, Novel perfluorinated nanofiltration membranes for isolation of pharmaceutical compounds, Sep. Purif. Technol., 258 (2021) 117944, doi: 10.1016/j.seppur.2020.117944.
[32] C. Wei, R. Qiang, L. Lin, Y. Gao, S. Ma, X. Zhang, X. Huang, Combing three-dimensional water channels and ultra-thin skin layer enable high flux and stability of loose polyimide/SiO_2 nanofiltration membranes at low operating pressure via one step in-situ modification, J. Membr. Sci., 623 (2021) 118944, doi: 10.1016/j.memsci.2020.118944.
[33] J. Yu, D. Froning, U. Reimer, W. Lehnert, Apparent contact angles of liquid water droplet breaking through a gas diffusion layer of polymer electrolyte membrane fuel cell, Int. J. Hydrogen Energy, 43 (2018) 6318–6330.
[34] T. Ahmad, C. Guria, A. Mandal, Optimal synthesis of high fouling-resistant PVC-based ultrafiltration membranes with tunable surface pore size distribution and ultralow water contact angle for the treatment of oily wastewater, Sep. Purif. Technol., 257 (2021) 117829, doi: 10.1016/j.seppur.2020.117829.
[35] B. Han, S. Liang, B. Wang, J. Zheng, X. Xie, K. Xiao, X. Wang, X. Huang, Simultaneous determination of surface energy and roughness of dense membranes by a modified contact angle method, Colloids Surf., A, 562 (2019) 370–376.
[36] C.-H. Liang, C. Li, T.-H. Chen, C.-Y. Cheng, C. Huang, Surface evaluation of reactive plasma-modified microporous polypropylene membrane by static contact angle analysis, Polym. Degrad. Stab., 160 (2019) 89–95.
[37] J. Chen, L. Shen, M. Zhang, H. Hong, Y. He, B.-Q. Liao, H. Lin, Thermodynamic analysis of effects of contact angle on interfacial interactions and its implications for membrane fouling control, Bioresour. Technol., 201 (2016) 245–252.